

Electrochemical Formation of Free-Standing 3D Structures Using Injection of Additives

Q. Huang, a,b,*,z R. Gyorgak, a and R. Pakc

A new method of electrochemical formation of free-standing 3D structures based on the injection of additives that controls the deposition rate was demonstrated using copper-chloride-polyethylene glycol as an example. A densely-packed defect-free pillar was formed upon the injection of chloride-free electrolyte into a chloride-containing electrolyte, where copper deposition was fully suppressed. The effects of diffusion coefficient, injection rate and the distance between injection nozzle and pillar top were evaluated with numerical simulation. A fast diffusion species, a moderate injection rate and a small gap between injection and pillar were found beneficial to obtaining the best contrast in the growth rates between pillar and background. The demonstration of free-standing copper structure in this paper provides an alternative path for electrochemical 3D printing of various metallic materials.

© The Author(s) 2017. Published by ECS. This is an open access article distributed under the terms of the Creative Commons Attribution Non-Commercial No Derivatives 4.0 License (CC BY-NC-ND, http://creativecommons.org/licenses/by-nc-nd/4.0/), which permits non-commercial reuse, distribution, and reproduction in any medium, provided the original work is not changed in any way and is properly cited. For permission for commercial reuse, please email: oa@electrochem.org. [DOI: 10.1149/2.1521712jes]

Manuscript submitted July 13, 2017; revised manuscript received August 16, 2017. Published August 31, 2017.

Free-standing metallic structures are of interest for various devices. The recently developed additive manufacturing enables the direct formation of such structures without the need of expensive lithography processes.¹ Among them, the metal wire feed process² was directly adapted from the original extrusion version of polymer 3D printing.^{3–5} Extrusion and sintering of metal paste⁶ also allow the formation of metal structures. Selective laser melting or sintering^{7–9} of metal particles can create free-standing or non-attached metallic structures embedded in metal powders.

All rights reserved.

While most of the above processes were heat-based physical processes, chemical reaction based 3D printing processes have been developed typically for direct formation of smaller structures. Tip based electrochemical machining has been widely used in the past to subtractively machine metallic or non-metallic structures for microdevices. ^{10,11} However, electrochemical deposition processes have not been used until more recently for additive formation of 3D metal ^{12–15} and conductive polymer ^{16–18} micro-structures.

Metal electrodeposition typically involves the reduction of metal ions into metal atoms on a conductive substrate. Therefore, 3D electrodeposition methods taking advantage of a local electrical field, local metal ion or local conductive substrate have been developed. The traditional lithography based electroforming, for example, the through-mask plating and LIGA process are based on the local exposure of conductive substrate. 19 This through mask concept has also been extended to achieve direct formation of nanostructures through local deposition.^{20–22} Another so-called local electrochemical deposition was invented relying on a locally positioned anode. 12-14 Such an anode is typically surrounded by a large insulating material and is closely positioned in a vicinity of the cathode substrate, ^{23–26} creating a highly local electrical field that enables the deposition to occur only at the location closest to the anode. Recently, Hirt et al.²⁷ used a modified atomic force microscope tip with fluidic channel to introduce metal electrolyte and demonstrated a controllable growth process for the local growth of 3D structures. In addition, a meniscus based electrodeposition process^{28–30} was also developed in a humidity controlled environment to enable 3D growth. This meniscus not only determines the local availability of metal ions but also confines the electric field.

This paper proposes and demonstrates an alternative method of 3D electrodeposition based on a contrast of reaction kinetics. While the electric field, metal ions and substrate were all universally available, a local distribution of additive molecules was used to control, i.e. suppress or promote, the deposition rate of metal. Such contrast in

the deposition rate results in the growth of 3D structures at certain locations while the deposition is suppressed at other places.

(cc) BY-NC-ND

Experimental

A home built computer controlled 3D stage with a stepsize of $1~\mu m$ was used to control the movement of substrate during 3D electrodeposition. The injection system comprised a LEGATO single syringe infusion pump, a HAMILTON micro-syringe and an injection tip at fixed position. The injection tip was formed from a borosilicate capillary tube using NARISHIGA pipette puller. A pulling procedure was developed to reproducibly pull the capillary tubes into micro-nozzles with an internal diameter of 15 μm . An optical microscope with up to 1000X magnification and 50 mm focal distance was used to enable in-situ observation of the nozzle as well as the growth of 3D structure. The stage, injection system and microscope were all built on an optical table to cancel any background vibration. An aluminum cabinet was built on the optical table to enclose everything and provide electrical shielding.

An Autolab PGSTAT electrochemical work station was used to carry out the electrochemical studies as well as the 3D structure growth. A glass container fixed on the 3D stage was used as the electrochemical cell. Five electrolytes were used in this study and their details are listed in Table I. For example, the copper deposition electrolytes contained 0.6 M CuSO₄, 0.1 M H₂SO₄, and various amounts of HCl and 300 ppm polyethylene glycol (PEG, average MW = 3,400). The pH of the solution, 0.5, was determined by the H₂SO₄ and the addition of HCl was negligible. A silicon coupon with an evaporated 100 nm gold layer was fixed in the glass cell and used as the cathode. Two copper strips were used as the anode and reference electrode. All electrodes were connected to the Autolab PGSTAT through a small opening on the aluminum shielding cabinet.

Numerical simulation was carried out with COMSOL multiphysics package. A JEOL 7000 scanning electron microscope (SEM)

Table I. Electrolytes used in the studies.

	CuSO ₄	H_2SO_4	HCl	PEG	pН	use
#1	0.6 M	0.1 M	varies	300 ppm	0.5	electrochemical studies
#2	0.6 M	0.1 M	0	300 ppm	0.5	injected
#3	0.6 M	0.1 M	30 ppm	300 ppm	0.5	background
#4	0.6 M	0.1 M	30 ppm	0	0.5	injected
#5	0	0.1 M	30 ppm	0	0.5	background

^aDepartment of Chemical and Biological Engineering, University of Alabama, Tuscaloosa, Alabama 35487, USA

^bCenter of Materials for Information Technology, University of Alabama, Tuscaloosa, Alabama 35487, USA

^cDepartment of Mechanical Engineering, University of Alabama, Tuscaloosa, Alabama 35487, USA

^{*}Electrochemical Society Member.

^zE-mail: qhuang@eng.ua.edu

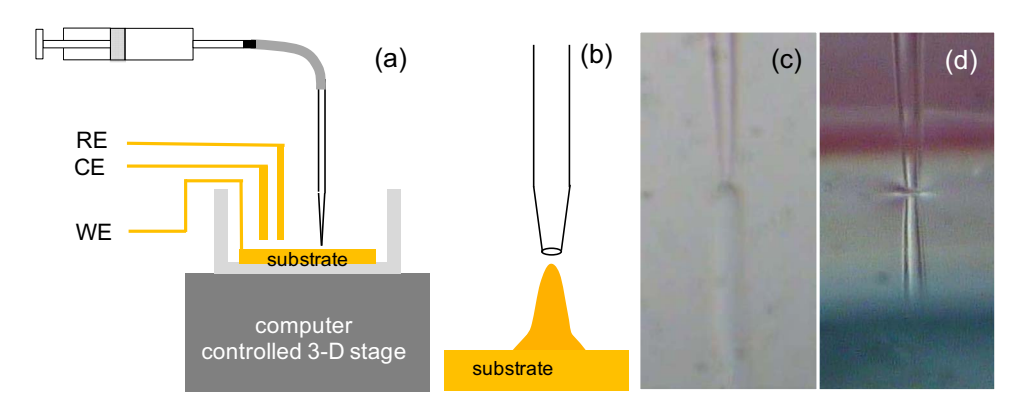


Figure 1. Diagrams of the (a) 3D deposition system and (b) the micro-injection nozzle, and optical images of an injection flow at 42 nL/min when the nozzle is positioned (c) in the electrolyte and (d) in vicinity of the substrate.

was used to characterize the 3D structure. The sample was first embedded in epoxy resin, diced, and then manually polished through a series of sand papers up to 1200 grits. The sample was finally polished with slurry with Al_2O_3 particles down to 50 nm diameter.

Results and Discussion

Figure 1 shows a diagram of the experimental setup. A regular electroplating cell comprising working electrode (cathode), counter electrode (anode) and reference electrode was secured on a computer controlled 3-D stage. The working electrode was attached to the cell to avoid any drift. A glass capillary with an inner diameter of about 15 μm was secured on a fixture and connected to a micro-injection pump. In order to avoid any volumetric variation in the pipelines due to bending, the positions of injection system and capillary are both fixed. Fluid injection rate was controlled with the pump. As illustrated in Figure 1b, while copper electrodeposition is suppressed everywhere in the solution the injected solution allows local copper deposition under the capillary. The relative position between nozzle and substrate was controlled by the 3-D stage.

Figure 1 also presents two optical micrographs of fluidic flow coming out of the nozzle. A steady laminar flow was observed in Figure 1c upon a 1 second high intensity injection pulse. Supporting material S1 shows the complete video of the same injection pulse. Flow started immediately upon the start of pulse, but the flow continued for more than 10 seconds after the pump stopped. Because of the small diameter and high aspect ratio of capillary tip, fluidic flow resistance was high. Flow immediately started as the pressure built up upon the rapid injection pulse. Yet the flow rate was limited by the fluidic resistance. As the flow continued after the pulse stopped, the fluidic pressure gradually decreased and the flow gradually diminished. Supporting material S2

shows the injection flow at a much slow rate of 4.2 nL/min. In this case, a gradual increase of the flow velocity was observed before a steady flow was achieved. Because of the slow injection, the pressure built up extremely slowly and the flow rate also increased gradually to achieve a steady state flow more than 20 seconds later. Figure 1d shows the injection flow when the nozzle was 20 μ m away from the substrate. A lateral dispersion of the injected flow was observed and a concentration variation on the substrate surface would be expected around the location under the injection nozzle.

While various organic additives have been studied in the past to alter the electrodeposition rates of metal elements, copper-chloridepolyethylene glycol (PEG) system^{31–33} was used in this study as a proof of concept. It is well known that the co-presence of both PEG and Cl⁻ suppresses copper deposition.^{34,35} Therefore, an electrolyte with PEG and Cl⁻ was used as the background electrolyte to suppress the background deposition. On the other hand, the choices of injected electrolyte can be PEG-free, Cl⁻-free or free of both. Figure 2 shows the simulated dimensionless concentration profiles of PEG and Clwhen an electrolyte free of those was injected through a 15- um diameter needle into a PEG or Cl⁻ containing electrolyte at an injection rate of 42 nL/min. A 50 μm tall 20 μm wide pillar is located under the needle across a 20 µm gap. The diffusion coefficients of Cl⁻ and PEG are 7E-5³⁶ and 5E-7³⁴ cm²/sec, respectively. The evolution of PEG concentration profile closely mimics the volume of the injected fluid. As the injection progresses, the PEG-free zone expands accordingly resulting in PEG free deposition at the foot of the pillar after 15 seconds. On the other hand, the Cl⁻-free zone is much smaller than PEG due to the much faster diffusion of Cl-. In addition, this Cl-free zone seems to reach a pseudo-steady state after only a fraction of second and does not grow much beyond the tip of pillar even after 15 seconds. Because a large contrast of the deposition rate between the

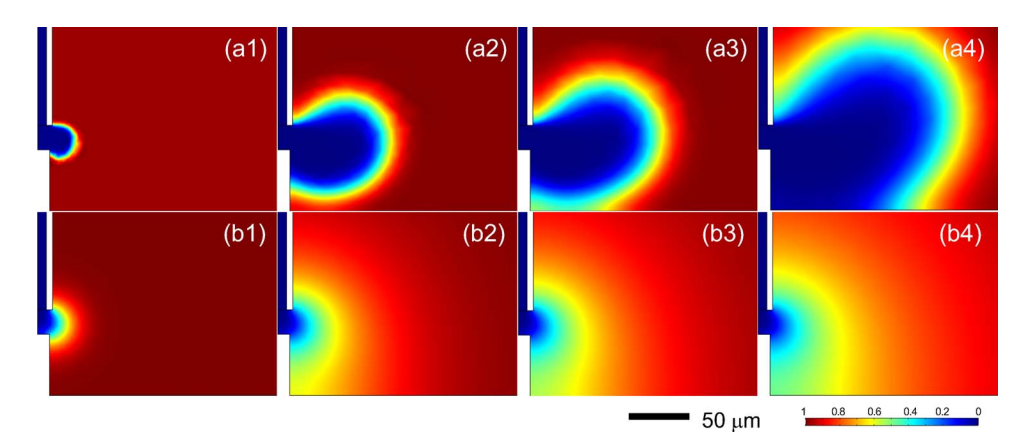


Figure 2. Simulated normalized concentration profiles of (a) PEG and (b) Cl at (a1, b1) 0.1, (a2, b2) 2.5, (a3, b3) 5, and (a4, b4) 15 seconds when a 0-concentration electrolyte is injected into a full concentration electrolyte on a 20 μm wide 50 μm tall pillar through a 15 μm diameter nozzle at an injection rate of 42 nL/min.

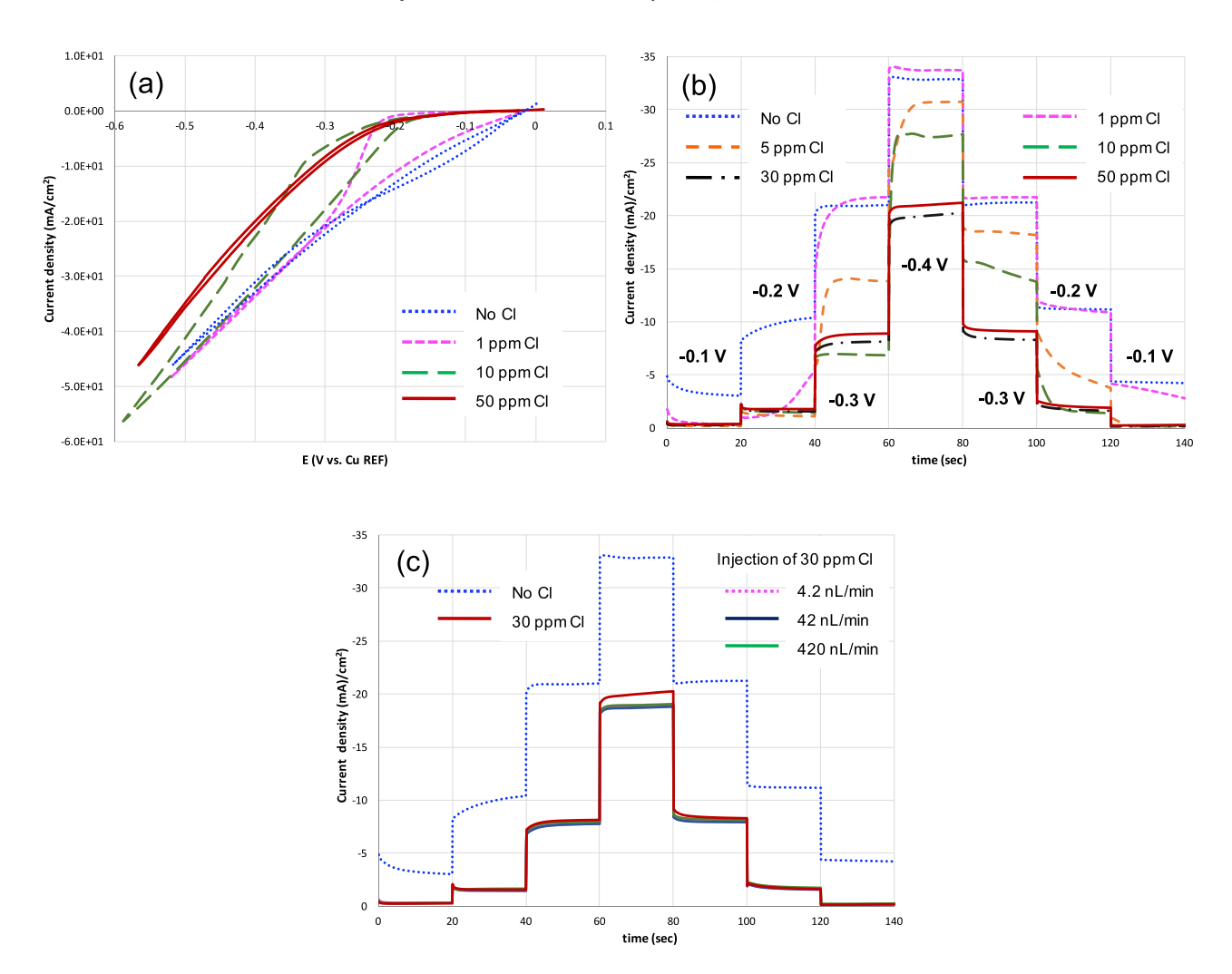


Figure 3. (a) Cyclic voltammetries and (b) pulsed amperometries of copper electrodeposition in bulk electrolytes with various chloride concentrations, and (c) the same pulsed amperometries of copper electrodeposition in electrolyte with 30 ppm Cl⁻ when the Cl⁻-free electrolyte was injected at different injection rates.

top and foot of pillar is desired for the formation of high aspect ratio 3D structures, injection of Cl⁻ free electrolyte is expected to be much more effective than injection of PEG-free electrolyte in creating such contrast.

Copper electrodeposition was studied in presence of 300 ppm PEG and various amounts of chloride. Figure 3a shows the cyclic voltammetry of the studies. With the addition of only 1 ppm Cl⁻ a significant suppression was observed between 0 to -0.22 V. However, this suppression does not hold at a more negative potential. In addition, such suppression was not present on the reverse sweep of CV, a known fact that the suppressing species on the copper surface was being incorporated into copper deposit, mitigating the suppressing effects.³⁷ With the addition of more Cl⁻, this suppression continues to higher potentials. A full suppression effect was observed at 50 ppm Cl⁻.

In order to find out the best contrast between deposition rates, deposition at different voltages with different amount of Cl^- was carried out and the results are presented in Figure 3b. The purpose of this study was to identify the optimal voltage that results in the most pronounced contrast in the deposition rates between Cl-free and fully suppressed cases. First, 30 ppm Cl^- resulted in full suppression of copper deposition and no difference was observed between 30 and 50 ppm cases for all the potentials studied. Second, while current transient behaviors were observed in some cases, such transients mostly do not continue beyond 20 seconds. In other words, steady state deposition behaviors were typically achieved within up to 20 seconds. Third, the ratio between the deposition rates in Cl-free and fully suppressed cases was the highest at -0.2 V for the potentials studied.

In addition, little copper deposition would occur even with as low as 1 ppm $\rm Cl^-$ if the potential is held at -0.2 V. This is expected to result in minimum background Cu deposition. While little suppression was observed in presence of 1 ppm at -0.3 V, significant suppression was reinstalled once the Cl concentration is beyond 5 ppm. Finally, the absolute difference between the deposition rates in Cl-free and 30-ppm Cl cases was, however, the largest at -0.3 V. This suggests that a 3-D structure would be formed fastest at -0.3 V. While this difference is approximately the same at a higher potential of -0.4 V, the background deposition at the fully suppressed state is much more significant. Therefore, 30 ppm $\rm Cl^-$ and a potential of -0.3 V will be used in further studies.

Copper electrodeposition was repeated again on a 4 mm x 5 mm substrate with the injection of Cl-free electrolyte (solution #2) into a fully suppressed electrolyte (30 ppm Cl, solution #3) at various injection rates. The bulk cases with 0 and 30 ppm Cl $^-$ were included for comparison. The injection rate of up to 420 nL/min (equivalent to a velocity of 40 mm/sec at the 15- μ m diameter nozzle) didn't result in any changes in the overall deposition current. This confirmed that the effect of injection was extremely local and its impact on deposition current was negligible for the overall deposition on the mm scale substrate.

While the contrast between deposition in presence of 0 and 30 ppm Cl has been maximized, the difference in Cl⁻ concentrations at the tip and foot of the pillar ultimately determine the growth behavior. Such difference was numerically calculated and the impacts of different operation conditions were evaluated. Figure 4a is a diagram showing

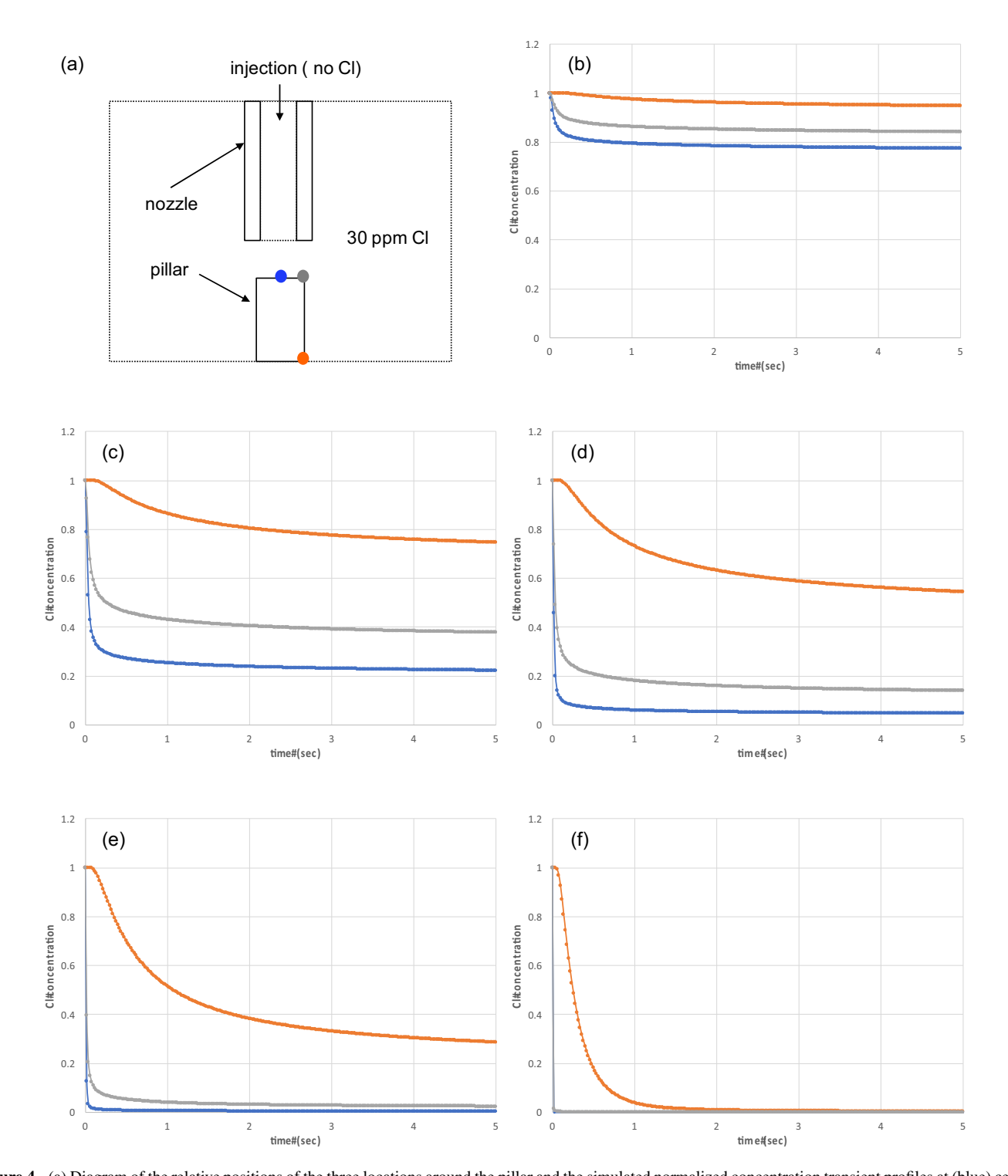
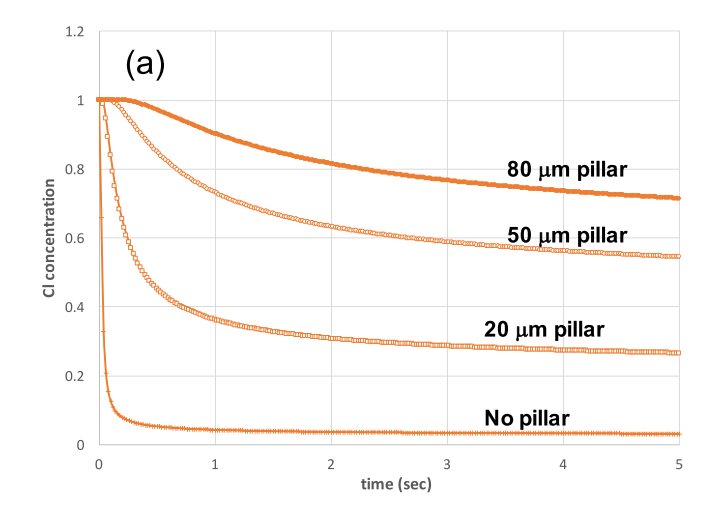


Figure 4. (a) Diagram of the relative positions of the three locations around the pillar and the simulated normalized concentration transient profiles at (blue) center of pillar top, (gray) corner of pillar top, and (orange) foot of pillar when a 0-concentration electrolyte is injected into a full concentration electrolyte through a 15 μm diameter nozzle placed above a 20 μm gap across a 20 μm wide 50 μm tall pillar at an injection rate of (b) 4.2, (c) 21, (d) 42, (e) 84 and (f) 420 nL/min.

the three locations where the Cl⁻ concentrations were calculated, the centre of pillar top, corner of pillar top, and corner of pillar foot.

Figures 4b to 4f shows five cases with different injection rates for a 50- μ m tall 20 μ m wide pillar that is under the injection nozzle across a 20- μ m gap. At an extremely slow injection rate, 4.2 nL/min, no Cl-free zone was created due to the fast diffusion of Cl. The Cl concentration remains at 80% of bulk concentration (24 ppm in this case) even at the centre of the pillar top. Therefore, copper deposition is expected to be almost fully suppressed everywhere. On the other

hand, the Cl concentration drops to 0 within 1 second even at the pillar foot when an extremely high injection rate, 420 nL/min, is used. In other words, no suppression is expected at such high injection rate and copper will be deposited uniformly within a wide area under the nozzle. When an intermediate injection rate is used, between 21 to 84 nL/min, a contrast in growth rate is resulted between the pillar top and foot. Among the three cases of 21, 42 and 84 nL/min, the 42 nL/min injection rate seemed to result in the most pronounced contrast between pillar top and foot. In addition, a nearly Cl-free



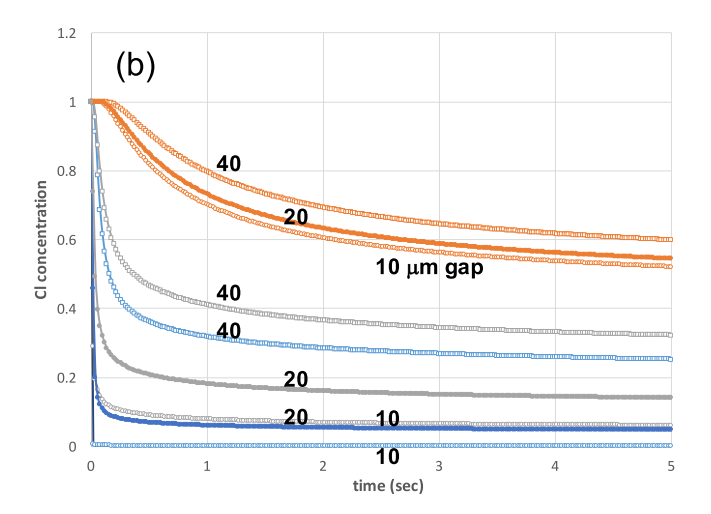


Figure 5. (a) Simulated normalized concentration transient profiles at (blue) center of pillar top, (gray) corner of pillar top, and (orange) foot of pillar when a 0-concentration electrolyte is injected into a full concentration electrolyte through a 15 μm diameter nozzle at an injection rate 42 nL/min through a nozzle of 15 μm diameter (a) placed at 20 μm above a pillar of various heights and (b) placed above a 50 μm tall pillar across a gap of various distance.

zone was maintained at the pillar top. The concentration at pillar foot stabilizes at about 55% of bulk concentration (16 ppm), which would be still fully suppressed at -0.3 V (Figure 3). A slower injection of 21 nL/min resulted in a steady state Cl concentration of 7 ppm and 11 ppm at the centre and corner of pillar top, respectively, which would significantly suppress the growth rate of pillar. On the other hand, 9 ppm Cl is present at the pillar foot after 5 seconds with an injection rate of 84 nL/min, which imposes a risk of significant background deposition or fattening of 3D structures. Therefore, an injection rate of 42 nL/min seemed to be optimal and was used in the following studies.

Similar simulations were also carried out to evaluate the impacts of pillar height and the gap between pillar and nozzle, which are presented in Figure 5. As the pillar grows little change was observed in the Cl concentration at the top of the pillar as long as the gap between nozzle and pillar is maintained. Figure 5a shows the concentration evolution at the foot of pillar, which increases as the pillar grows taller. This is consistent with the expectation that the impact of injection diminishes because it becomes further away from the pillar foot. At a pillar height of 80 μm , the Cl concentration at the pillar foot stays above 70% of bulk concentration, which is believed to maintain a fully suppressed deposition rate.

On the other hand, the gap between injection nozzle and pillar top has little to no impact on the Cl concentration at the foot. It has a rather strong impact on the concentration at the pillar top. As the injection nozzle is further away from the pillar top, the Cl-free zone is also moved further upwards. The concentration at the pillar top increases due to the diffusion from the bulk electrolyte. Therefore, the deposition will be more suppressed when the injection nozzle moves away from pillar top. In other words, controlling this gap distance between injection nozzle and pillar is expected to be critical to maintaining a constant and fast growth rate of 3D structures. As shown in Figure 5b, the smaller this gap is, the larger the concentration difference is between the top and foot of pillar, the faster the pillar grows. However, an extremely small gap is difficult to maintain. We have not yet set up an automatic control feedback loop for this gap in this demonstration. A 20-µm gap was used with a constant stage movement speed.

There are some other parameters in the process that might impact the overall growth behavior of such directly formed pillar structure. Diameter of the nozzle not only relates to the flow velocity at the nozzle but also determines the diameter of pillar. Nozzles with a fixed size (15 μm) was used in this study with a corresponding pillar diameter of 20 μm . Viscosity is expected to impact not only the flow behavior but also the diffusion of metal ions and additives. However, dilute solutions at room temperature was used in this study and the viscosity is considered as a constant and the same as water.

A demonstration of the formation of a pillar was carried out at a potential of -0.3 V with an injection of 42 nL/min Cl-free electrolyte (solution #2) into 30-ppm Cl electrolyte (solution #3). The nozzle was kept at about 20 µm above the pillar. As shown in Figure 6, a 780 µm tall pillar was formed with 2 hour deposition. The animation of the in-situ observation of pillar growth is presented in Supporting Material S3. From the electrochemical investigation (Figure 3), the deposition current density in absence of Cl and agitation was 21 mA/cm², equivalent to a deposition rate of 0.47 μm/min. However, the growth rate of the pillar was more than 13 times higher, at about 6.5 μm/min. This is believed due to the increased Cu²⁺ diffusion because of the injected flow as well as the spherical geometry of the diffusion toward the micro-tip of the pillar. The background copper growth depends on the strength of suppression for this particular suppressor system, Cl-PEG. The deposition current density in presence of 30 ppm Cl without agitation was 8.1 mA/cm², equivalent to a deposition rate of $0.18 \,\mu$ m/min or $22 \,\mu$ m for 2 hours. The Cu film at the base of pillar was about 40 µm thick, suggesting a slightly increased deposition rate than the stationary case in Figure 3. In addition, the pillar was about 101 μ m in diameter at the foot and about 20 μ m at the top, consistent with the 40 µm widening during the course of 2 hour deposition. While this fattening of pillar, or background deposition, is not desired for 3D structure formation, it can be mitigated or avoided when a strong suppressor is used in the background electrolyte. It can also be mitigated when a less negative potential is used for electrodeposition in the sacrifice of deposition rate (Figure 3). The surface of the pillar was relatively smooth and the cross-section SEM analysis shows the dense defect-free structure of pillar.

The lateral growth of the pillar at the foot depends on the local chloride concentration, which relates to the inject rate of Cl-free solutions. Two experiments were carried out to verify the effects of injection rates predicted by simulation (Figure 4). At an extremely low injection rate of 4.2 nL/min, the chloride concentration is expected to remain the same as the background solution at both the top and foot, resulting in no growth contrast. Deposition was carried out at -0.3V (vs. Cu REF) and 4.2 nL/min for 5700 seconds. SEM inspection did not show any pillar growth. On the other hand, at an extremely high injection rate of 420 nL/min, Cl concentration was predicted to drop to 0 quickly. This results in a fast deposition on the sidewall. The structure formed at this condition for 1500 seconds is shown in Figure 7a. The diameter was 97 μ m at the pillar top and 314 μ m at the foot. The significant growth of the diameter at foot was consistent with the prediction from the simulation in Figure 4. In addition, the injected solution dispersed in the lateral direction once reaching the pillar top,

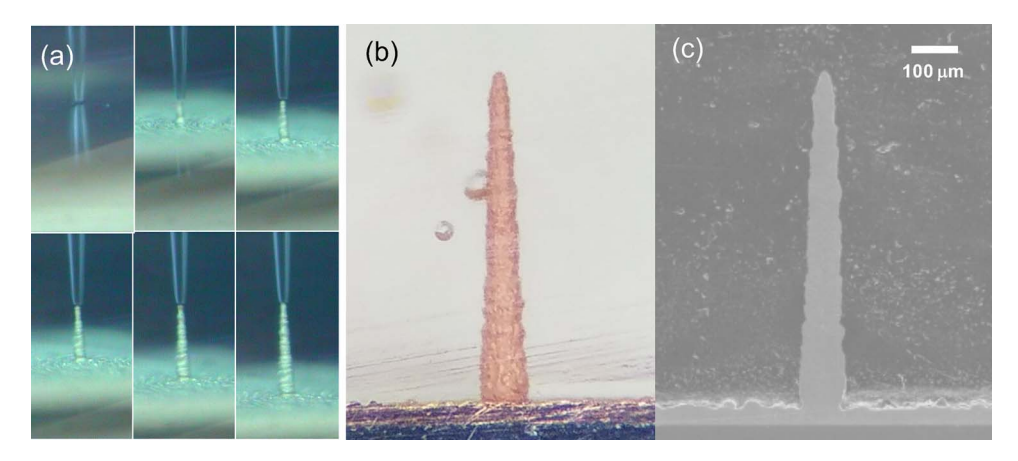


Figure 6. (a) In situ observation of the growth of a copper pillar upon the injection of Cl⁻-free electrolyte into an electrolyte with 30 ppm Cl⁻ at a rate of 42 nL/min, and the (b) optical observation and (c) cross sectional SEM observation of the pillar.

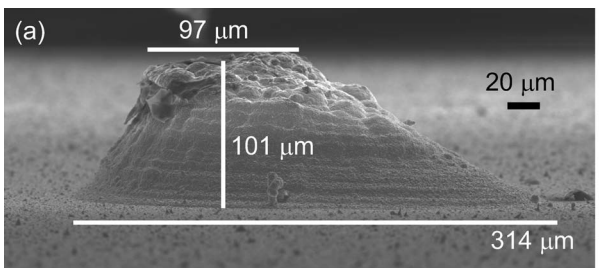




Figure 7. (a) SEM image of a structure formed at -0.3 V (vs. Cu) upon the injection of Cl⁻-free electrolyte into an electrolyte with 30 ppm Cl⁻ at a rate of 420 nL/min and (b) diagram of a tilted injection nozzle explaining the asymmetric shape of the structure.

resulting in significantly larger diameter (than the nozzle) at the pillar top. Because of a small tilting of the injection nozzle with respect to the substrate explained in Figure 7b, an asymmetric structure was obtained. One side of the pillar grew much wider than the other side due to the asymmetric dispersion of injected electrolyte. While this tilting of nozzle was also present during the formation of pillar in Figure 6, its effect was not observed at the slow injection rate. Formation of a true 3D structure is demonstrated in Supporting Material S4, where a vertical sickle-shaped structure was deposited and significant growth on sidewall was also observed.

As a comparison to the pillar in Figure 6, a copper pillar was also deposited with injection of Cu^{2+} -containing electrolyte (solution #4) into a Cu^{2+} -free electrolyte (solution #5). In this method, 3D metal structure forms because of the local availability of the metal cations. A same potential of $-0.3\ V$ and same injection rate of 42 nL/min were also used. While the pillar grew much faster than the previous case (1000 μm for 30-minute deposition, in Figure S5), Figure 8a shows

a much rougher dendritic surface. The pillar was not mechanically strong and slightly slanted during the clean-dry process due to the surface tension of water. The cross-sectional SEM also confirmed a dendritic and porous internal structure of pillar. The poor connectivity between dendritic islands was consistent with the macroscopic poor mechanical strength.

The growth rate of the pillar in Figure 6, 6.5 µm/min, was relatively slow in comparison with the millimetre size of the structure being produced and a higher growth rate would be desired. While increasing applied potential is expected to further increase the deposition rate at the tip of the pillar (Figure 3), the background deposition will also increase, which may diminish the net growth rate of the pillar. However, an improved chemistry system that suppresses metal deposition more strongly at even higher potentials would enable faster growth of the 3D structure at higher potential. In addition, while copper was used in this study as a demonstration, additives that suppress the deposition of other metals have been reported in some other studies^{38–44} and

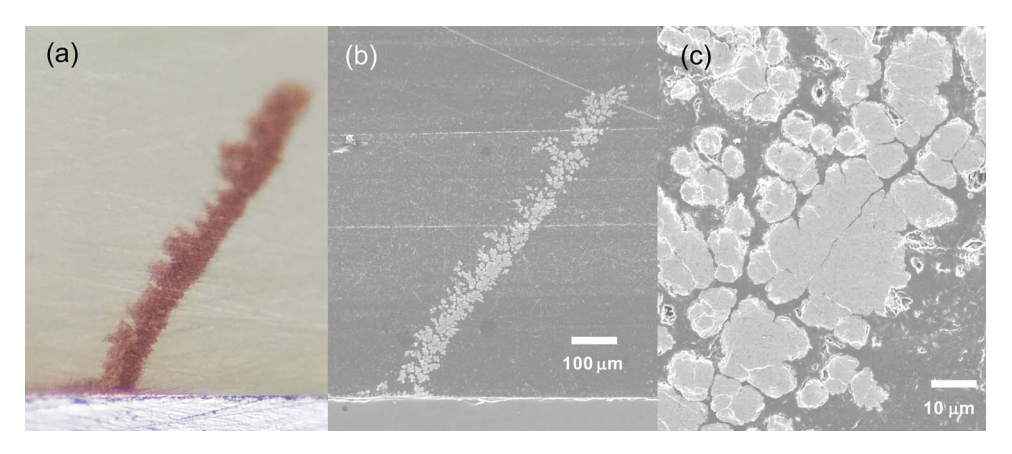


Figure 8. (a) Optical observation and (c) cross sectional SEM observation of a pillar grown upon the injection of an electrolyte with $0.6 \,\mathrm{M}\,\mathrm{Cu}^{2+}$ into a Cu^{2+} -free electrolyte at $42 \,\mathrm{nL/min}$. (b) the zoomed in cross sectional SEM image showing the poor continuity of pillar.

are believed to enable such 3D growth of free-standing structures as well.

Conclusions

A new electrodeposition method to form free-standing 3D metal structures based on the injection of additives was proposed, evaluated, and demonstrated using copper-Cl-PEG system. The injection of chloride free electrolyte through a micro-nozzle into a fully suppressed electrolyte with 30 ppm chloride resulted in local copper deposition under the nozzle. Electrochemical studies on blanket substrates showed the optimal deposition rate contrast was obtained at a potential of -0.3 V. Numerical simulation not only predicted that the fast diffusion of Cl limits the Cl-free zone around the tip of the pillar, but also suggested the injection of PEG-free electrolyte will not be idea due to its slower diffusion and a much larger and faster-growing PEG-free zone. Furthermore, an injection rate of 42 nL/min was predicted to be optimal, enclosing the pillar top in the Cl-free zone while avoiding significant dilution of the Cl at the pillar foot. While this Cl concentration at the pillar foot increases as the pillar grows and the nozzle moves upwards, the gap between pillar top and nozzle has little impact on this concentration. However, a smaller gap is beneficial to the concentration difference and therefore the deposition rate difference between the top and foot of pillar.

A comparison was carried out between two free-standing pillars formed with the two methods of injecting Cl-free electrolyte into 30 ppm Cl electrolyte and of Cu electrolytes into Cu-free support electrolyte. While a dense defect free pillar was obtained in the former case, the copper pillar deposited with the later method was dendritic with an extremely rough surface. The injection of Cl was used here as an example to control deposition kinetics of copper. But this demonstration is believed to open up different opportunities for a variety of additives for different metals or alloys.

Acknowledgment

National science foundation is acknowledged for support through grant CMMI-1662332. This study was also supported by the Research grant Council (RGC) at the University of Alabama (UA) through grant RG-14741. UA mechanical shop and UA central analytical facility are greatly acknowledged for making mechanical parts for the 3D experiment setup and for instrumental access used in SEM characterization, respectively.

References

- 1. W. E. Frazier, Journal of Materials Engineering and Performance, 23, 1917 (2014).
- 2. K. M. Taminger, K. J. Watson, R. A. Hafley, and D. D. Petersen, US Pat. No. 7,168,935 (2007).
- 3. S. S. Crump, US Pat. No. 5121329 (1992).
- 4. S. S. Crump, US Pat. No. 5340433 (1994).

- 5. S. S. Crump, US Pat. No. 5503785 (1996).
- 6. B. Y. Ahn, E. B. Duoss, M. J. Motala, X. Guo, S. I. Park, Y. Xiong, J. Yoon, R. G. Nuzzo, J. A. Rogers, and J. A. Lewis, Science, 323, 1590 (2009).
- 7. C. R. Deckard, US Pat. No. 4,863,538 (1989).
- 8. J. J. Beaman and C. R. Deckard, US Pat. No. 4,938,816 (1990).
- D. L. Bourell, H. L. Marcus, J. W. Barlow, J. J. Beaman, and C. R. Deckard, US Pat. No. 4,944,817 (1990).
- 10. S. Roy, J Phys D Appl Phys, 40, R413 (2007).
- 11. A. P. Malshe, K. P. Rajurkar, K. R. Virwani, C. R. Taylor, D. L. Bourell, G. Levy, M. M. Sundaram, J. A. McGeough, V. Kalyanasundaram, and A. N. Samant, Cirp Ann-Manuf Techn, 59, 628 (2010).
- 12. J. D. Madden and I. W. Hunter, Journal of microelectromechanical systems, 5, 24
- 13. I. W. Hunter, S. R. Lafontaine, and J. D. Madden, US Pat. No. 5641391 (1997).
- 14. J. D. Whitaker, J. B. Nelson, and D. T. Schwartz, J Micromech Microeng, 15, 1498 (2005).
- 15. J. B. Nelson and D. T. Schwartz, J Micromech Microeng, 15, 2479 (2005).
- 16. S. S. Shiratori, S. Mori, and K. Ikezaki, Sensors and Actuators B: Chemical, 49, 30 (1998)
- 17. J. Liu and M. Wan, Journal of Materials Chemistry, 11, 404 (2001).
- 18. Y. Yang and M. Wan, Journal of Materials Chemistry, 11, 2022 (2001).
- 19. L. T. Romankiw, *Electrochim Acta*, 42, 2985 (1997).
- 20. S. Kitayaporn, J. H. Hoo, K. F. Bohringer, F. Baneyx, and D. T. Schwartz, Nanotechnology, 21, 195306 (2010).
- 21. S. Abbasi, S. Kitayaporn, D. T. Schwartz, and K. F. Bohringer, Nanotechnology, 22, 165303 (2011).
- 22. S. Abbasi, S. Kitayaporn, M. J. Siedlik, D. T. Schwartz, and K. F. Bohringer, Nanotechnology, 23, 305301 (2012).
- 23. A. Jansson, G. Thornell, and S. Johansson, J Electrochem Soc, 147, 1810 (2000).
- 24. T. Chang, J. Lin, J. Yang, P. Yeh, D. Lee, and S. Jiang, J Micromech Microeng, 17,
- 25. C.-Y. Lee, C.-S. Lin, and B.-R. Lin, J Micromech Microeng, 18, 105008 (2008).
- 26. M. M. Sundaram, A. B. Kamaraj, and V. S. Kumar, J Manuf Sci E-T Asme, 137, 021006 (2015).
- 27. L. Hirt, S. Ihle, Z. Pan, L. Dorwling-Carter, A. Reiser, J. M. Wheeler, R. Spolenak, J. Voros, and T. Zambelli, *Advanced Materials*, 28, 2311 (2016).
 J. Hu and M. F. Yu, *Science*, 329, 313 (2010).
- 29. S. K. Seol, D. Kim, S. Lee, J. H. Kim, W. S. Chang, and J. T. Kim, *Small*, 11, 3896 (2015).
- 30. K. Y. Scott, A. Halajko, and G. G. Amatucci, J New Mat Electr Sys, 18, 25 (2015).
- 31. J. P. Healy, D. Pletcher, and M. Goodenough, Journal of electroanalytical chemistry(1992, 338, 155 (1992).
- 32. J. Kelly and A. West, Journal of The Electrochemical Society, 145, 3472 (1998).
- 33. J. Kelly and A. West, Journal of The Electrochemical Society, 145, 3477 (1998)
- 34. R. Akolkar and U. Landau, Journal of The Electrochemical Society, 151, C702 (2004). 35. P. Broekmann, A. Fluegel, C. Emnet, M. Arnold, C. Roeger-Goepfert, A. Wagner,
- N. T. M. Hai, and D. Mayer, *Electrochimica Acta*, 56, 4724 (2011).
- 36. W. M. Haynes, CRC Handbook of Chemistry and Physics, 97th ed, CRC Press (2016).
- 37. M. Hayase, M. Taketani, K. Aizawa, T. Hatsuzawa, and K. Hayabusa, Electrochemical and Solid-State Letters, 5, C98 (2002).
- 38. S. Kim, D. Josell, and T. Moffat, Journal of The Electrochemical Society, 153, C616 (2006).
- 39. S. Kim, J. Bonevich, D. Josell, and T. Moffat, Journal of The Electrochemical Society, 154, D443 (2007).
- 40. D. Josell, M. Silva, and T. P. Moffat, Journal of The Electrochemical Society, 163, D809 (2016)
- 41. D. Josell and T. Moffat, Journal of The Electrochemical Society, 163, D322 (2016).
- 42. D. Liang, J. Liu, K. Reuter, B. Baker-O'Neal, and Q. Huang, Journal of the Electrochemical Society, 161, D301 (2014).
- 43. Q. Huang, T. Lyons, and W. Sides, Journal of The Electrochemical Society, 163, D715 (2016)
- 44. T. Lyons and Q. Huang, Electrochimica Acta, 245, 309 (2017).